Biophysical Journal Volume 83 July 2002 229–241

Cloning and Expression of the Human T-Type Channel $Ca_v3.3$: Insights into Prepulse Facilitation

Juan Carlos Gomora, Janet Murbartián, Juan Manuel Arias, Jung-Ha Lee, and Edward Perez-Reyes
Department of Pharmacology, University of Virginia, Charlottesville, Virginia 22908 USA

ABSTRACT The full-length human $Ca_v3.3$ (α_{1I}) T-type channel was cloned, and found to be longer than previously reported. Comparison of the cDNA sequence to the human genomic sequence indicates the presence of an additional 4-kb exon that adds 214 amino acids to the carboxyl terminus and encodes the 3′ untranslated region. The electrophysiological properties of the full-length channel were studied after transient transfection into 293 human embryonic kidney cells using 5 mM Ca^{2+} as charge carrier. From a holding potential of −100 mV, step depolarizations elicited inward currents with an apparent threshold of −70 mV, a peak of −30 mV, and reversed at +40 mV. The kinetics of channel activation, inactivation, deactivation, and recovery from inactivation were very similar to those reported previously for rat $Ca_v3.3$. Similar voltage-dependent gating and kinetics were found for truncated versions of human $Ca_v3.3$, which lack either 118 or 288 of the 490 amino acids that compose the carboxyl terminus. A major difference between these constructs was that the full-length isoform generated twofold more current. These results suggest that sequences in the distal portion of $Ca_v3.3$ play a role in channel expression. Studies on the voltage-dependence of activation revealed that a fraction of channels did not gate as low voltage-activated channels, requiring stronger depolarizations to open. A strong depolarizing prepulse (+100 mV, 200 ms) increased the fraction of channels that gated at low voltages. In contrast, human $Ca_v3.3$ isoforms with shorter carboxyl termini were less affected by a prepulse. Therefore, $Ca_v3.3$ is similar to high voltage-activated Ca^{2+} channels in that depolarizing prepulses can regulate their activity, and their carboxy termini play a role in modulating channel activity.

INTRODUCTION

Molecular cloning studies have identified 10 genes encoding the pore-forming α_1 subunits of voltage-gated calcium channels. Analysis of their deduced amino acid sequences revealed that they could be grouped into three subfamilies, which also coincided with their pharmacological and biophysical properties (Ertel et al., 2000). Low voltage-activated (LVA), T-type, Ca^{2+} channels are referred to as the Ca_v3 family. The last member of this family to be cloned was $Ca_v3.3$, or α_{1I} (Lee et al., 1999). Biophysical analysis of the cloned channel revealed that it was an LVA channel; however, it had a very different kinetic profile from that recorded from either native tissues (Huguenard, 1996) or the other cloned T-type channels $Ca_v3.1$ (α_{1G}) and $Ca_v3.2$ (α_{1H}) (Cribbs et al., 1998; Perez-Reyes et al., 1998). Notably, it activated and inactivated much more slowly, suggesting that it plays a different role in neuronal excitability (Kozlov et al., 1999). Slow T-type channels have been found in neurons isolated from the rat nucleus reticularis (Huguenard and Prince, 1992), lateral habenula (Huguenard et al., 1993), laterodorsal thalamic nucleus (Tarasenko et al., 1997), and rod bipolar cells (Pan, 2000). In situ hybridization studies support the hypothesis that these slow T-type channels are encoded by $Ca_v3.3$ (Talley et al., 1999).

The human gene encoding $Ca_v3.3$, CACNA1I, is on chromosome 22 (22q13.1). Sequencing of this gene by the Wellcome Trust Genome Campus allowed PCR cloning of parts of both a rat cDNA (Lee et al., 1999) and a human cDNA (Monteil et al., 2000b). PCR cloning of the 5′ and 3′ ends is critically dependent on the method used to identify the coding regions. In this study we report the existence of an additional exon that encodes the final 214 amino acids of the carboxyl terminus and 3333 bp of the 3′ untranslated sequence. A full-length cDNA was cloned (LT9) and expressed in 293 cells. The electrophysiological properties were then compared to truncated versions of $Ca_v3.3$ (LT4 and LT6), and to $Ca_v3.1$ and $Ca_v3.2$. Methods for measuring channel activation were optimized, revealing a second population of channels that required stronger depolarizations for opening. A strong prepulse could convert these channels back to low-voltage-activated channels. Human $Ca_v3.3$ isoforms with shorter carboxyl termini were less affected by a prepulse. A preliminary report of these findings has appeared in abstract form (Gomora et al., 2000).

Submitted October 23, 2001, and accepted for publication April 3, 2002.

Address reprint requests to Edward Perez-Reyes, Ph.D., Department of Pharmacology, University of Virginia Health System, P.O. Box 800735, 1300 Jefferson Park Ave., Charlottesville, VA 22908-0735. Tel.: 804-982-4440; Fax: 804-982-3878; E-mail: eperez@virginia.edu.

Juan Carlos Gomora's present address is Departamento de Biofísica, Instituto de Fisiología Celular, UNAM, México DF 04510, México.

Jung-Ha Lee's present address is Department of Life Science, Sogang University, Shinsu-dong, Mapo-gu, Seoul 121-742, Republic of Korea.

0006-3495/02/07/229/13 $2.00

MATERIALS AND METHODS

Cloning of the human $Ca_v3.3$ cDNA

Human brain cDNA libraries derived from either fetal brain or cerebellum (Clontech, Palo Alto, CA) were screened using the rat $Ca_v3.3$ as probe (Lee et al., 1999). Screening was done by filter hybridization according to the manufacturer's protocol. The cDNA probes were synthesized using ^{32}P-α-dCTP and a commercial labeling kit (Life Technologies, Rockville,

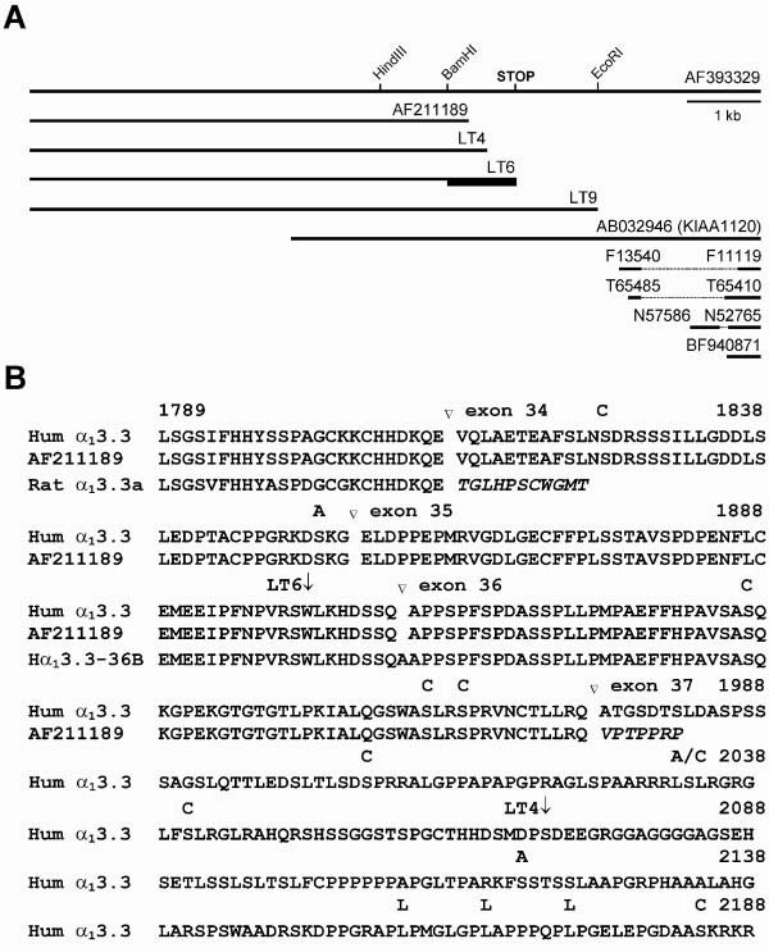

FIGURE 1 Cloning of distinct isoforms of the $Ca_v3.3$ subunit of T-type Ca^{2+} channels. (*A*) Schematic representation of the clones and restriction enzyme sites used to generate the constructs LT6 and LT9. The top line represents the size of the mature mRNA. The thick part of the line representing LT6 corresponds to the fragment amplified by PCR. Also shown are the locations of EST clones and their GenBank accession numbers. (*B*) Alignment of the deduced amino acid sequence of the novel human sequence reported herein (Hum $\alpha_1$3.3) to published sequences of either the human AF211189 (Monteil et al.; 2000b or the rat $Ca_v3.3a$ (Lee et al., 1999. Only the carboxyl termini are shown, with the alignment beginning at residue 1789 and ending at the stop codon. The IVS6 segment ends at residue 1696, so there are an additional 93 aa of the carboxyl terminus not shown. Exons are numbered as originally proposed (Mittman et al., 1999). The rat CACNA1I gene appears to have similar intron/exon boundaries in this part of the gene. Our original rat clone contains DNA sequences that are 78% identical to exons 34 through 37. The coding region of rat $Ca_v3.3a$ ends prematurely because exon 34 is spliced in a different reading frame (see (Monteil et al., 2000b)). Preliminary observations indicate that rats also splice exon 34 as humans, generating a carboxy terminus that is the same length as LT9 and 85% identical (Murbartián et al., 2002). The human clone AF211189 was cloned by PCR; the 3′ PCR primer was located in what we suggest is the intronic sequence after exon 36 (Monteil et al., 2000b). The amino acids that differ between the isoforms are shown in italics. The arrows indicate where the coding regions of clones LT4 and LT6 terminate. Consensus phosphorylation sequences for protein kinase A are noted above the sequence with the letter A, while those for protein kinase C are noted with the letter C. Also noted is a leucine zipper motif (L). PCR detected a variant that contains an extra 3 bp at the exon 36 boundary (H$\alpha_1$3.3–36B), which encodes an alanine. The nucleotide sequence of the full-length cDNA can be accessed through the GenBank with accession number AF393329.

MD). Positive clones were plaque purified, then subcloned into pUC18 for sequencing. A BLAST (Altschul et al., 1997) search of the GenBank with the rat $Ca_v3.3$ identified the genomic DNA encoding the human CACNA1I gene (GenBank AL022312), allowing us to design PCR primers to clone the 5′ end. Overlapping clones were selected and ligated in the vector pcDNA3 (Invitrogen, Carlsbad, CA), generating the clone LT4 (Gomora et al., 2000). A BLAST search using the sequence of our most 3′ clone (HM1) led to the identification of an additional exon in the human genome (GenBank HS172B20), and the clone KIAA1120 (GenBank AB032946).

Two approaches were used to extend LT4. One, the missing 1.2-kb fragment, was amplified by PCR using the forward primer GCC GGC TGC AAG AAG TGT CA and the reverse primer CAG GTG TGG ACG AAG TAT TG. This fragment was subcloned, and nine clones were partially sequenced. All nine clones spliced exon 35 to 36 so that an additional three bases were added, which encodes an alanine residue ($\alpha_1$3.3–36B), and all spliced exon 36 to 37, as shown for $\alpha_1$3.3 in Fig. 1. The *Bam*HI (5657)/*Not*I (polylinker) fragment from clone 2 was ligated to *Hind*III- and *Not*I-digested pcDNA3 vector and two LT4 fragments: *Hind*III (polylinker)/*Hind*III (4750) and *Hind*III (4750)/*Bam*HI (5657). Sequencing of the resulting plasmid, LT6, revealed a nonsense mutation that would result in a truncated protein. This mutation was only observed in one of six products subcloned from this PCR reaction, indicating that it was an artifact. In the second approach the missing fragment was derived from AB032946. The full-length cDNA (LT9) was constructed by ligating the *Hind*III (polylinker)/*Hind*III (4750) fragment of LT4 to the *Hind*III (4750)/*Eco*RI (7721) fragment of AB032946. Both LT6 and LT9 were constructed with a version of pcDNA3 that had been modified to contain 54 bp of the 5′ untranslated region of *Xenopus* β-globin. Previous studies have shown that this sequence can significantly enhance expression in *Xenopus* oocytes (Liman et al., 1992), and does not interfere with expression in mammalian cells (Lee et al., 1999). Injection of *Xenopus* oocytes with cRNA synthesized from the LT9 construct led to robust expression of I_{Ba} (>5 μA; results not shown).

PCR

Two additional PCR experiments were used to test for alternative splicing at the exon 36–37 borders. The first experiment contained three reactions: 1) upper primer u3 (GGA GAC CTG GGC GAA TGC TTC) and the reverse primer am1 (TTA GAT CCT GCC CCT TGC CC); 2) upper primer u4 (GCA CCC CCA AGT CCC TTC TCC) and am1; 3) upper primer u3 and the reverse primer r16 (GGG GCT GTC GCT CAG GGT CAG). The sequence and utility of the am1 primer was reported previously (Monteil et al., 2000b). PCR primers were purchased from Operon (Alameda, CA). The second experiment used a nested PCR strategy where the first reaction (PCR-1) used the primers u3 and r16. This product was purified on QIAquick columns (Qiagen, Valencia, CA), and then used as template for PCR-2. PCR-2 reactions used the primer sets u4-r16 and u4-am1. PCR was performed in a Mastercycler (Eppendorf, Westbury, NY) using 1 unit of

Taq DNA polymerase (Eppendorf) according to the manufacturer's protocol. The PCR with the am1 primer used an annealing temperature of 61°C, and all others at 63–64°C. The temperature cycle consisted of 25-s incubations for denaturation (94°C), annealing, and extension (72°C). The cycle was repeated 45 times except for PCR-2, which had 35 cycles. The template was human cerebellum Marathon-ready cDNA (Clontech).

Transfections

Human embryonic kidney 293 cells (CRL-1573, American Type Culture Collection, Manassas, VA) were transiently co-transfected with plasmid DNA for green fluorescent protein (GFP) and LT9, LT6, or LT4 by the calcium phosphate method (CalPhos Maximizer Transfection Kit, Clontech) according to the manufacturer's protocol. After ~24 h GFP-positive cells were selected for electrophysiological recordings. Similar methods were used to generate stably transfected cell lines, except GFP was omitted. Cells were selected using 1 mg/ml G418 (Life Technologies). Two cell lines were generated for this study: LT9–8, which was transfected with the LT9 construct of $Ca_v3.3$; and Hh8–5, which was transfected with the Hh8 construct of $Ca_v3.2$. The Q-31 cell line that expresses $Ca_v3.1a$ has been reported previously (Cribbs et al., 2000).

Electrophysiology

Electrophysiological experiments of 293 cells were carried out using the whole-cell configuration of the patch clamp technique. Recordings were obtained from two different set-ups. One set-up consisted of an Axopatch 200B amplifier, Digidata 1200 A/D converter, and pCLAMP 8.0 software (Axon Instruments, Union City, CA). The second set-up used an Axopatch 200A amplifier, Digidata 1200 A/D converter, and pCLAMP 6.0 software (Axon Instruments). Data were generally filtered at 5–10 kHz by the amplifier, and then digitized at 4 kHz. Tail currents were nominally filtered at 10 kHz and digitized at 50 kHz. Whole-cell Ca^{2+} currents were recorded using the following external solution (in mM): 5 $CaCl_2$, 155 tetraethyl ammonium (TEA) chloride, and 10 HEPES, pH adjusted to 7.4 with TEA-OH. The internal pipette solution contained the following (in mM): 125 CsCl, 10 EGTA, 2 $CaCl_2$ (free Ca^{2+} = 28 nM), 1 $MgCl_2$, 4 Mg-ATP, 0.3 Na_3GTP, and 10 HEPES, pH adjusted to 7.2 with CsOH. Pipettes were made from TW-150–6 capillary tubing (World Precision Instruments, Inc., Sarasota, FL), using a model P-97 Flaming-Brown pipette puller (Sutter Instrument Co., Novato, CA). Under these solution conditions the pipette resistance was typically 2–3 MΩ. Series resistance values ranged between 2 and 10 MΩ (4.3 ± 0.3, n = 88) and were compensated between protocols to at least 70%. Cell capacitance was measured using the Membrane Test function (Axon Instruments). Average cell capacitance was 10.9 ± 0.6 pF (n = 88). All experiments were performed at room temperature (22–24°C).

Data analysis

Peak currents and exponential fits to currents were determined using Clampfit 8.0 software (Axon Instruments). Leak subtraction was performed off-line using the passive resistance algorithm in Clampfit. Activation and inactivation kinetics were fit simultaneously because at some voltages inactivation is only twofold slower than activation. The beginning of the fit range was set to a time where the current was inward (typically 3 ms), thereby excluding an initial outward transient that may represent gating currents, and any associated lag (see Fig. 3 *C*). The voltage dependence of activation was estimated using two methods. One method is based on chord conductances, and uses the following equation to fit normalized *I-V* data: $G = G_{max} \cdot (V_m - V_{rev})/(1 + \exp((V_{1/2} - V_m)/k)$, where G is conductance, V_m is the test potential, V_{rev} is the apparent reversal potential, $V_{1/2}$ is the midpoint of activation, and k is the slope factor. This method has been used extensively, and we use it to allow direct comparisons to these studies. Due to nonlinear permeation near the reversal potential, this method underestimates activation. Therefore, only the data obtained during test potentials below +20 mV were fit with this equation. A second method using tail currents is also described, and these data were fit with a double Boltzmann equation of the form $Y = A/(1 + \exp((V_{1/2} - V_m)/k) + (1 - A)/(1 + \exp((V_{1/2}' - V_m')/k')$, where A represents the fraction of current activating with the first component. The software program Prism (GraphPad, San Diego, CA) was used to generate the graphs and calculate statistics. The current-voltage and steady-state inactivation curves were fit for each cell then averaged. Average data are presented as mean ± SEM. Statistical tests included unpaired two-tailed Student's t-tests for comparing two data sets and the F-test for comparing two models such as single- or double-exponential fits.

RESULTS

Cloning of the human $Ca_v3.3$ cDNA

Human brain cDNA libraries were screened using the cDNA encoding the rat α_1 subunit of the T-type channel $Ca_v3.3$ (α_{1I} or $\alpha_1 3.3$) as probe (Lee et al., 1999). Overlapping clones were ligated in the vector pcDNA3, generating clone LT4 (Fig. 1). The 3′ sequence of this clone extends further than previously published sequences of human $Ca_v3.3$ (Mittman et al., 1999; Monteil et al., 2000b). A BLAST search using the sequence of the most 3′ clone (HM1) led to the identification of an additional exon in the human genome (GenBank AL022319). This exon is 3969 bp long, and encodes the final 214 amino acids of the carboxy terminus (Fig. 1 *B*). According to the numbering of exons suggested by Mittman et al., this exon would be no. 37 (Mittman et al., 1999). A polyadenylation signal (AATAAA) is present 17 bp before the end of the clone. Five lines of evidence support the conclusion that exon 36 is spliced directly to exon 37 in most $Ca_v3.3$ mRNA transcripts. First, inclusion of exon 37 would create an mRNA of ~10 kb (6.5 kb coding plus 3.3 kb untranslated), while its omission would create one of just 6.5 kb. Northern analysis detects a predominant transcript of ~10–11 kb, but no 6.5 kb transcripts (Lee et al., 1999; McRory et al., 2001; Monteil et al., 2000b). Second, a BLAST search with the new exon 37 sequence identifies 19 ESTs whose 3′ end is at the 3′ end of exon 37, but none that end at exon 36. Eight of these are from rat, six from mouse, one from pig, and five from human. The human clones are distinct, as they were cloned from four distinct cDNA libraries (Fig. 1). Third, a BLAST search with the intron between exons 36 and 37 fails to detect any ESTs, indicating that this intron is efficiently removed. Fourth, no product was detected when PCR used either of two forward primers in exon 36 (u3, u4) and the previously reported reverse primer (Monteil et al., 2000b), herein called am1 (results not shown). In contrast, a product of the correct size is amplified if the reverse primer (r16) is located in exon 37 (Fig. 2). Fifth, we next considered the possibility that some transcripts might contain both the intron between exon 36 and 37, and exon 37, resulting in an ~11 kb mRNA. Although such a transcript

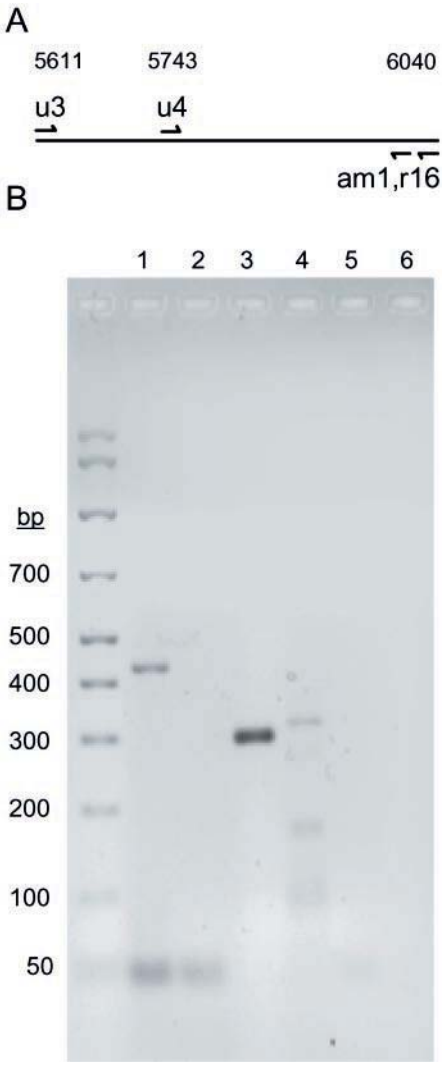

FIGURE 2 PCR detection of exon 36 and 37 splicing events. (*A*) Schematic representation of the PCR strategy. Numbers refer to the location of the primers in the AF393329 sequence, with the exception of am1, which is not present in AF393329. Primer sequences are reported in Methods. (*B*) PCR products after separation in an agarose gel and staining with ethidium bromide. A nested PCR strategy was used where the product shown in lane 1 (7 μl of u3-r16), was used in a second PCR to generate the products shown in lanes 3 (1 μl of u4-r16) and 4 (10 μl of u3-am1). No template controls that would detect possible contamination of the reagents are shown in lane 2 (7 μl of u3-r16), lane 5 (5 μl of u4-r16), and lane 6 (5 μl of u4-am1). Molecular weight standards and their sizes are shown on the left.

should have been amplified in the previous PCR, we decided to increase the sensitivity by using a nested PCR strategy (Fig. 2 *A*). PCR-1 used primers in exons 36 (u3) and 37 (r16). This product was purified, and then an aliquot was used in PCR-2. Again, a product was readily detected when the primers were located in exons 36 (u4) and 37 (r16). In contrast, only a very faint band of the correct size was detected using u4 and am1 primers. Fig. 2 shows 1 μl of the u4-r16 product, and 10 μl of the u4-am1 products. From this we conclude that the u4-r16 product is at least 1000 times more abundant than the u4-am1 product. We suggest that am1 is located in an intron, and that PCR can detect incompletely spliced transcripts. We also suggest that neither our clone LT4 nor the cDNA constructed by Monteil et al. (see Fig. 1) were full-length (Monteil et al., 2000b). We cloned the missing fragment with PCR, ligated it to LT4, thereby generating the clone LT6. Subsequent sequencing revealed that the fragment generated by PCR contained a nonsense mutation in the codon encoding tryptophan at residue 1901. Thus, the protein encoded by LT6 is missing 288 amino acids, and is even shorter than LT4, which is missing 118 residues. To clone a cDNA that contained the entire coding sequence (LT9), we ligated the *Hind*III (polylinker)/*Hind*III (4750) fragment of LT4 to the *Hind*III (4750)/*Eco*RI (7721) fragment of AB032946.

Electrophysiological characterization of the full-length $Ca_v3.3$

The electrophysiological properties of the full-length $Ca_v3.3$ Ca^{2+} channel encoded by LT9 were compared to those observed with the truncated channels LT4 and LT6 using transiently transfected 293 cells and the whole cell configuration of the patch clamp technique. We also studied the properties of LT9 in a stably transfected cell line (LT9−8), and compared these properties to those of human $Ca_v3.1$ and $Ca_v3.2$ (Table 1). Representative Ca^{2+} currents generated by LT9 and LT4 are compared in Fig. 3. The electrophysiological behavior of LT6 channels was nearly identical to those observed with LT4 and LT9 (Table 1). Currents were elicited by 500-ms depolarizing steps in 10-mV increments from a holding potential of −100 mV. All three channels produced typical T-type currents, displaying a low threshold for activation (−70 mV), and voltage-dependent kinetics that produce a criss-crossing pattern (Randall and Tsien, 1997). One clear difference between the recombinant channels was that LT9 generated larger currents. To eliminate the size of the cells as a variable, the peak current amplitude (I) at each potential was divided by the membrane capacitance (C_m) of each cell and the resulting ratio (current density, in pA/pF) was plotted against test potential (V_m; Fig. 3 *A*). Current density was significantly higher in cells expressing LT9 than in those transfected with either LT6 or LT4. Using the currents generated during test pulses to −30 mV, their current density (pA/pF) was the following: LT9, -111 ± 14, $n = 35$; LT6, -81 ± 13, $n = 31$; and LT4, -50 ± 6, $n = 24$, $p < 0.0001$).

Inward currents generated from all Ca_v3 recombinant channels started to be detectable at −70 mV, and peaked near −30 (Fig. 3 *B*). The apparent reversal potential for all channels was +40 mV. The inward currents were carried by Ca^{2+} (5 mM), while the outward currents were carried by Cs^{+} (125 mM) (Lee et al., 1999; Serrano et al., 1999). The voltage-dependence of activation can be calculated from

TABLE 1 Summary of the electrophysiological properties of currents from human Ca_v3 channels

	$Ca_v3.3$						
	AF211189[†]	LT4	LT6	LT9	LT9-8	$Ca_v3.2$	$Ca_v3.1$
Activation							
Peak of *I-V* curve (mV)	−24	−30	−30	−30	−30	−30	−30
$V_{1/2}$ (mV)	−40.6 ± 0.3 (11)**	−43.9 ± 2.0 (7)	−42.7 ± 2.7 (6)	−44.9 ± 1.5 (9)	−41.8 ± 0.7 (9)**	−43.7 ± 0.7 (10)**	−45.2 ± 2.2 (8)**
Slope (*k*; mV)	5.6 ± 0.1 (11)**	6.3 ± 0.3 (7)	6.4 ± 0.4 (6)	6.0 ± 0.3 (9)	5.9 ± 0.2 (9)	6.1 ± 0.1 (10)*	5.4 ± 0.2 (8)**
Inactivation							
$V_{1/2}$ (mV)	−68.9 ± 0.9 (8)**	−70.8 ± 1.8 (5)	−73.3 ± 1.7 (5)	−71.5 ± 1.1 (6)	−72.0 ± 0.9 (7)	−78.8 ± 0.7 (7)**	−76.9 ± 1.9 (3)**
Slope (*k*; mV)	−5.6 ± 0.1 (8)**	−5.2 ± 0.2 (5)	−5.8 ± 0.3 (5)*	−5.0 ± 0.2 (6)	−5.7 ± 0.2 (7)*	−5.3 ± 0.2 (7)	−4.7 ± 0.2 (3)*
Kinetics at −50 (τ; ms)							
Activation	66 ± 4 (24)	35 ± 6 (7)**	38 ± 6 (6)	43 ± 3 (9)	53 ± 5 (9)**	9.9 ± 0.4 (10)**	8.2 ± 0.9 (8)**
Inactivation rate	273 ± 24 (7)**	179 ± 33 (7)**	155 ± 34 (6)	126 ± 22 (9)	127 ± 14 (9)	28 ± 3 (10)**	62 ± 23 (8)**
Kinetics at −30 (τ; ms)							
Activation	20 ± 1 (26)	16 ± 4 (7)	17 ± 3 (6)	14 ± 1 (9)	17 ± 1 (9)**	3.8 ± 0.1 (10)**	2.9 ± 0.4 (8)**
Inactivation rate	96 ± 4 (21)**	94 ± 9 (7)**	75 ± 8 (6)	80 ± 5 (9)	70 ± 5 (9)**	16 ± 1 (10)**	17 ± 6 (8)**
Kinetics at −10 (τ; ms)							
Activation	10 ± 1 (19)	6 ± 1 (7)	6 ± 1 (6)	5.9 ± 0.5 (9)	6.2 ± 0.3 (9)	1.8 ± 0.1 (10)**	1.1 ± 0.1 (8)**
Inactivation rate	89 ± 3 (21)**	90 ± 9 (7)*	73 ± 7 (6)*	80 ± 5 (9)	68 ± 5 (9)**	15 ± 1 (10)**	16 ± 1 (8)**
Recovery from inact. (ms)	297 ± 44 (11)	233 ± 7 (7)	238 ± 16 (6)	257 ± 19 (7)	286 ± 7 (7)	415 ± 38 (7)**	65 ± 3[§] (3)**
Deact. kinetics at −90 (ms)	1.2 ± 0.1 (25)**	2.1 ± 0.2[‡] (3)	2.1 ± 0.2[‡] (4)	2.0 ± 0.2[‡] (6)	1.8 ± 0.2[‡] (8)	2.6 ± 0.3 (4)**	2.1 ± 0.1[§] (8)

The properties of the full-length $Ca_v3.3$ construct LT9 were compared to those obtained with the truncated constructs LT4 and LT6, and to the reported properties of AF211189 (Monteil et al., 2000b). Statistically significant differences are noted if the *P* value was <0.05 (*) or <0.01 (**). LT9 currents obtained from transiently transfected cells were compared to those obtained in the stably transfected cell line LT9-8, and the significance is noted, also shown are values obtained from representative members of each Ca_v3 subclass recorded from stably transfected cells. The cell line expressing $Ca_v3.2$ was Hh8-5, and the $Ca_v3.1$ line was Q-39. $Ca_v3.1$ and 3.2 values were compared to those obtained with the cell line LT9-8, and the significance is noted. Data are expressed as mean values ± SE. The number of cells are reported in parentheses.

[†]Data from Monteil et al. (2000b); recorded using 2 mM Ca^{2+} as charge carrier, and kinetics of activation were reported as 10–90% rise time.

[‡]Weighted tau.

[§]Data from Cribbs et al. (2000); recorded using 10 mM Ba^{2+}.

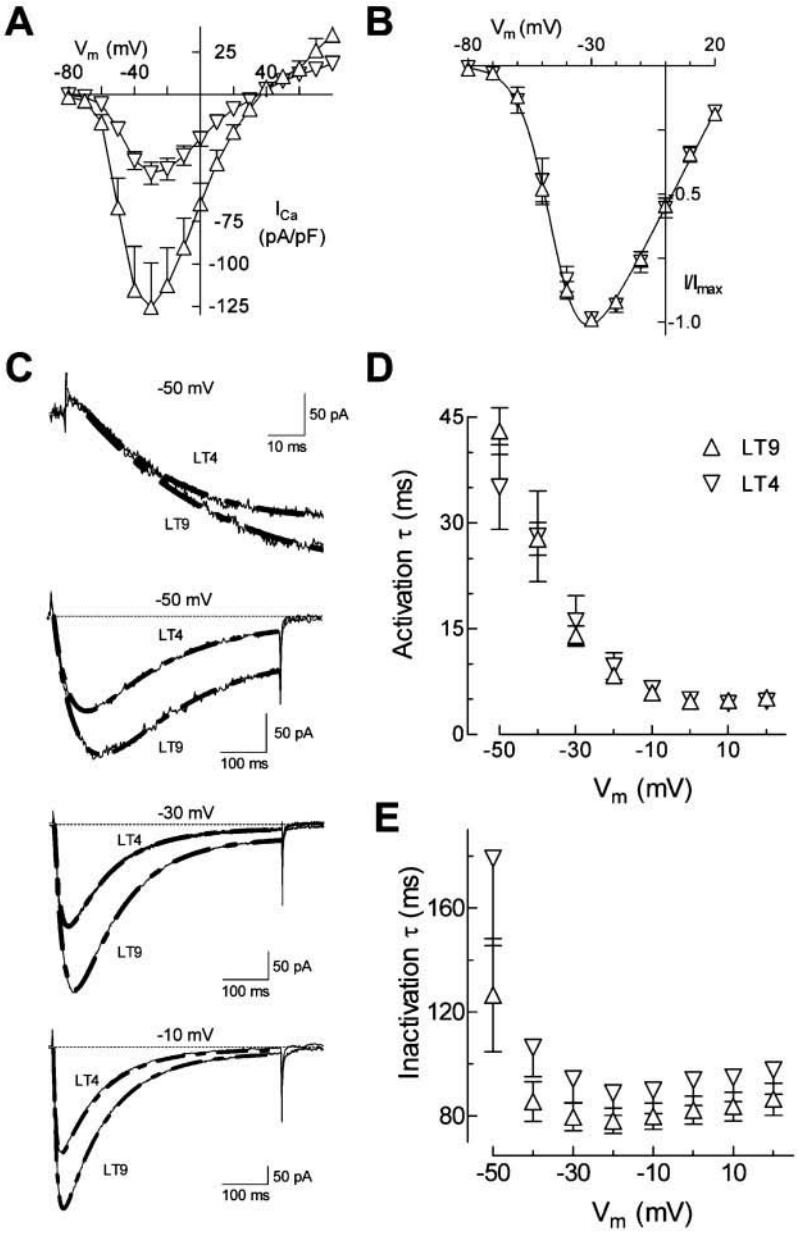

FIGURE 3 Voltage-dependence of channel opening. (*A*) Average *I-V* relationships for LT9 ($n = 12$), and LT4 ($n = 7$). Data points show peak current density (mean ± SE) at each potential. (*B*) *I-V* data were normalized to the maximum peak current density for each cell, and then averaged. The solid line shows the fit to the average data obtained using a Boltzmann function that takes into account changes in driving force (see Methods). (*C*) Representative whole-cell Ca^{2+} currents obtained from 293 cells transiently transfected with human $Ca_v3.3$ clones LT9 and LT4. Recordings were acquired at 10-s intervals in response to 500-ms depolarizing pulses of 10 mV steps (V_m) from a holding potential of −100 mV. Traces were filtered at 5 kHz. Dotted lines represent double-exponential fits to the inward currents. (*D*) Activation and (*E*) inactivation tau (τ) values are plotted as a function of test potential for human $Ca_v3.3$ channels. Data points ($n = 10$ for LT9, *triangles*; $n = 11$ for LT4, *inverted triangles*) are the average time constants obtained from two exponential fits of currents as shown in (*C*).

normalized *I-V* data (Fig. 3 *B*) using a modified Boltzmann function that accounts for changes in the driving force (see Methods). The midpoint of activation ($V_{1/2}$) of LT9 channels was −45 mV and the slope factor was −6.4, and the values obtained with either LT4 or LT6 were not significantly different (Table 1). Similar results were obtained with $Ca_v3.1$ and $Ca_v3.2$ in stably transfected cells. LT9 channels in the stable cell line gated at slightly more negative potentials, but this effect was modest (−3 mV).

The activation and inactivation kinetics of the human $Ca_v3.3$ channels were studied using the same 500-ms pulses used to measure the *I-V*. Current recordings were fit with two exponentials, one for activation and the second for inactivation (Fig. 3 *C*). The average time constants are shown in Fig. 3, *D* and *E*. Activation kinetics of all $Ca_v3.3$ channels were slow near threshold (~40 ms at −50 mV), but faster and essentially voltage-independent for membrane potentials above −20 mV (~5 ms). Similarly, inactivation was relatively slow near threshold, but faster and voltage-independent during test pulses above −40 mV. The voltage-independent inactivation τ was ~80 ms. The truncated constructs LT4 and LT6 had similar kinetics, although at some potentials they were significantly different (Fig. 3, *D* and *E*; Table 1). Significantly slower inactivation kinetics were reported with AF211189 (Table 1) in 2 mM Ca^{2+} (Monteil et al., 2000b). Similar properties were also observed using a stably transfected cell line expressing LT9 (LT9−8), although activation and inactivation were faster

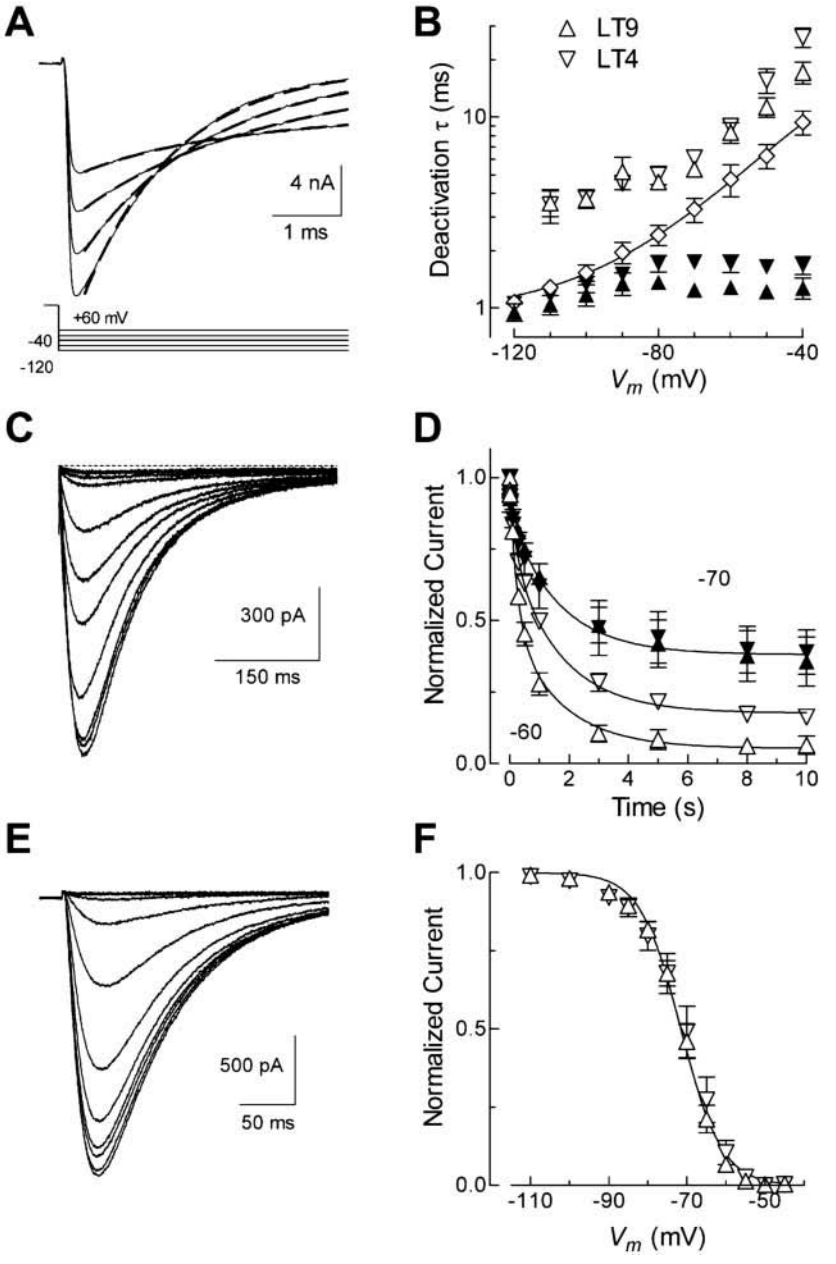

FIGURE 4 Deactivation and inactivation of human $Ca_v3.3$ channels. (*A*) Representative tail currents obtained from a 293 cell transiently transfected with LT9. For clarity, the protocol has been truncated to show only the last 1 ms of the 10-ms depolarization at +60 mV, and the first 5 ms of the 50-ms repolarization. Tail currents were well fit with two exponentials (*dotted lines*). The fit region began 0.34 ms after repolarization from +60 mV. (*B*) Dependence of the deactivation time constants on repolarization potential (V_m). Data points ($n = 12$ for LT9, *triangles*; and $n = 16$ for LT4, *inverted triangles*) are the two time constants, which represent the fast (*filled symbols*) and slow components of the tail (*open symbols*). Also shown is the weighted τ for LT9 (*diamonds*), which was derived using the equation $\tau = A_1\tau_1 + A_2\tau_2$, where A_1 and A_2 are the normalized amplitude of the fast and slow component. (*C*) Representative family of LT9 currents elicited by test pulses to −30 mV after varying periods at −60 mV. (*D*) Average time course of inactivation measured at either −60 mV (*open symbols*) or −70 mV (*filled symbols*). Data points show the average of four cells. Solid lines are fits to the sum of two exponentials. (*E*) Voltage-dependence of steady-state inactivation. Channels were inactivated by 15-s conditioning pulses to potentials between −110 and −40 mV (V_m), and then channel availability was tested by a voltage step to −30 mV. Shown are representative currents recorded at −30 mV from a cell expressing human LT9 channels. (*F*) Average data obtained for LT9 and LT4. The solid line shows the fit to the LT9 data with a Boltzmann function.

(Table 1). $Ca_v3.1$ and $Ca_v3.2$ channels activate and inactivate much faster.

Closing channels from the open state leads to a tail current. The kinetics of this deactivation process were studied by repolarizing the membrane to different voltages after a 10-ms step to +60 mV. Sample tail currents and the protocol are shown in Fig. 4 *A*. Recent studies indicate that rat $Ca_v3.3$ tail currents close in a biexponential manner (Frazier et al., 2001). Similarly, the human $Ca_v3.3$ tail currents were fit better to two exponentials (Fig. 4 *A*). For example, at a repolarization potential of −90 mV, LT9 currents decayed with a fast τ of 1.3 ± 0.2 and a slow τ of 5 ± 1 ms. The fast component predominates at this and more negative potentials (<−100 mV), while the slow component steadily increases at less negative potentials. This shift is illustrated by the voltage dependence of the weighted τ ($A_{fast}\tau_{fast} + A_{slow}\tau_{slow}$), which is similar to the fast τ below −100 mV, then closer to the slow τ above −70 mV (Fig. 4 *B*). LT4 (Fig. 4 *B*) and LT6 (Table 1) deactivated with kinetics similar to LT9. Similar results were obtained in stably transfected cell lines, with the exception of $Ca_v3.2$, which deactivated more slowly.

The development of inactivation was measured using prepulses of varying duration to either −60 or −70 mV, followed by a test pulse to −30 mV. Representative traces obtained with LT9 are shown in Fig. 4 *C*. Experimental data

sets were better fit with two exponentials than one (LT9, −70 mV: $F = 7.5$, $p = 0.02$), and all could be fit with time constants of 0.6 and 4 s. A greater proportion of LT9 channels inactivated at −60 mV with the slow time constant relative to −70 mV. Although LT9 and LT4 behaved similarly at −70 mV, at −60 mV a greater fraction of LT9 channels inactivated with the slow time constant (52% vs. 27%), and to a greater extent than LT4 (93% vs. 77%, $p < 0.05$). These results indicate that the minimum time required to reach steady-state inactivation (h_∞) is 10 s. Therefore, we studied the voltage dependence of inactivation using 15-s prepulses followed by a 300-ms pulse to −30 mV to test channel availability (Fig. 4 *E*). Each experimental data set was normalized to the peak current obtained after the −110 mV prepulse, then fit to a Boltzmann function (Fig. 4 *F*). LT9, LT6, LT4, and LT9 in the stable cell line inactivated with a similar voltage dependence: $V_{1/2} \sim -72$ mV, $k = -5.4$. In contrast, $Ca_v3.1$ and $Ca_v3.2$ inactivated at more negative voltages (Table 1).

Recovery from short-term inactivation (500-ms pulse to −30 mV) was measured with a multistep protocol where the time between the inactivating pulse and the test pulse was varied (Fig. 5 *A*). Prompted by a study describing a lag in the recovery of thalamic T-type currents (Kuo and Yang, 2001), we performed a similar analysis where the small residual current at the end of the inactivating pulse was subtracted from both the control and the recovered current. For LT9 the residual current was 4% of the peak current. Recovery was then defined as the ratio of recovered current divided by the current that inactivated during the conditioning pulse (Fig. 5 *B*). No significant recovery of current was observed when the interpulse interval was 5 ms or less (Fig. 5 *C*), which is similar to what was observed with native channels. Recovery could be well-fit by a single exponential with a time constants ranging from 233 ms for LT4 to 257 ms for LT9 (Fig. 5 *B*; Table 1). Somewhat surprisingly, the current recovered to a value slightly greater than control (after 2 s, $I/I_{control} = 1.07 \pm 0.03$, $n = 8$ LT9, $p < 0.05$). This suggests that the first pulse not only inactivated channels, but also induced facilitation. As observed with the rat isoforms (Klöckner et al., 1999), each Ca_v3 isoform recovers from short inactivating pulses with distinct kinetics, with $Ca_v3.2$ being slower, and $Ca_v3.1$ being faster than $Ca_v3.3$ (Table 1).

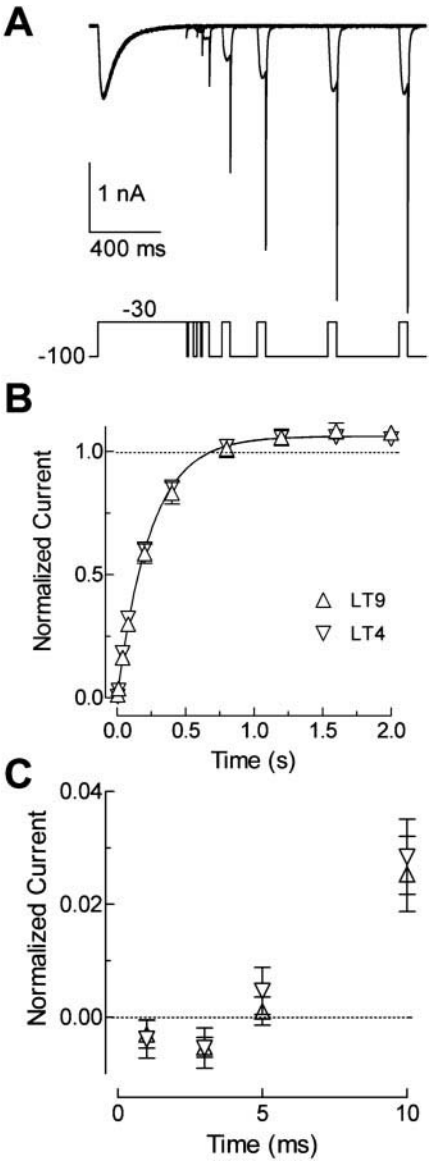

FIGURE 5 Recovery from inactivation. (*A*) Representative traces showing how a 500-ms pulse to −30 mV inactivated Ca^{2+} currents, which were then allowed to recover at −100 mV for periods ranging from 1 to 2000 ms, then tested during a 30-ms voltage step to −30 mV. Recordings were filtered at 5 kHz. (*B*) Average recovery data for LT4 and LT9 ($n = 7$). The kinetics of recovery for the two channels were not significantly different, so the data were fit to the average (260 ms). (*C*) Expanded time scale to show that there was little recovery after 1, 3, and 5 ms at −100 mV.

Other techniques for measuring the voltage dependence of activation

A recent study of rat $Ca_v3.3$ channels indicated that activation was less voltage-dependent and occurred at more positive potentials than previously estimated from *I-V* data (Frazier et al., 2001; Lee et al., 1999). The use of *I-V* data underestimates activation near the reversal potential due to nonlinear permeation. Some studies of the voltage dependence of native T-type Ca^{2+} channels have used the amplitude of slowly deactivating tail currents after test pulses of varying amplitude to estimate activation (Huguenard and Prince, 1992). Because tail currents are recorded at a single voltage, this method is not influenced by nonlinear permeation. Typically, the test pulses are of fixed duration, which tends to underestimate activation at threshold potentials. To circumvent this problem, Monteil et al. studied activation using pulses of varying duration based on the time-to-peak of the cloned $Ca_v3.1$ (Monteil et al., 2000a). To apply this

method to $Ca_v3.3$ we first determined the time-to-peak from data taken during the *I-V* protocol (Fig. 6 *A*). The time-to-peak was voltage-dependent during negative test potentials, then reached an apparent plateau around 5 ms. A peak was difficult to ascertain for traces obtained near the reversal potential; therefore, we estimated these values by extrapolation. Typical traces obtained with this protocol are illustrated in Fig. 6 *B*. Average tail amplitudes for LT9 channels are shown in Fig. 6 *C*. Tail current amplitudes continued to increase until the depolarizing pulse reached +130 mV. The data were normalized to the maximum observed, then fit to the sum of two Boltzmann functions (see Fig. 7 *C*). The low-threshold component activated with a similar voltage dependence ($V_{1/2} = -35.3 \pm 0.8$, $k = 8.7 \pm 0.7$), as observed for the normalized *I-V*, while the second component activated at much higher potentials ($V_{1/2} = 52 \pm 4$, $k = 28 \pm 2$).

A prepulse alters voltage dependence of activation

High voltage-activated channels of the Ca_v2 family also activate in two modes, which have been termed willing and reluctant (Bean, 1989). G-proteins inhibit channel gating by shifting channels to the reluctant mode, and a strong depolarizing pulse can overcome this. Therefore, we decided to test whether a similar prepulse could affect gating of LT9 (Fig. 7 *A*). In contrast to the control (labeled pp off), tail current amplitudes after a prepulse appeared to saturate at much lower voltages for both channels (pp on, Fig. 7 *B*). Fits to the normalized data suggest that the fraction of channels gating in LVA mode increased from 54 to 65% (Fig. 7 *C*). To illustrate this effect, current traces are shown in Fig. 7 *A* that have been normalized to the maximum tail current. Note that the tail current after repolarization from +10 mV is proportionally larger after a prepulse. This stimulation was ~35% between −40 and +40 mV, then decreased at higher potentials (see Fig. 8 *C*). Because this assay relies on the time-to-peak, any change in kinetics could possibly affect the results. Fig. 7 *D* shows that the prepulse did not affect the activation kinetics of the inward currents elicited during the test pulse. In contrast, the outward currents were significantly faster after a prepulse.

Similar studies using LT4 and LT6 also revealed the presence of a second population of channels activating at positive potentials (Fig. 8; $V_{1/2} = 17 \pm 4$ mV, $k = 24 \pm 1$). In contrast to LT9, the gating of LT6 was much less affected by a prepulse ($p < 0.001$). Representative traces are shown in Fig. 8 *A*. The prepulse had only a small effect on the normalized tail current after depolarization to +10 mV (Fig. 8, *B* and *C*). The average maximum stimulation induced by the prepulse followed the order LT9 (33.8 ± 0.6%, $n = 7$) > LT4 (19.4 ± 0.4%, $n = 8$) > LT6 (8.5 ± 0.4%, $n = 6$).

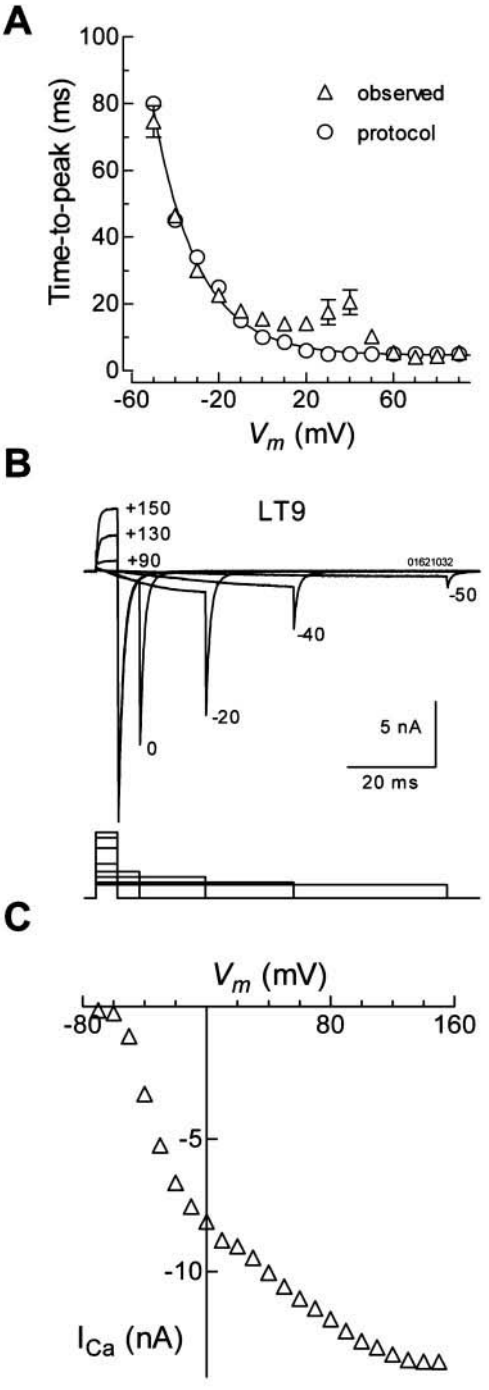

FIGURE 6 Voltage dependence of activation measured using tail currents. (*A*) The time-to-peak was calculated from data obtained for LT9 during the *I-V* protocol (see Fig. 3). Average data were plotted as a function of the test potential (V_m). True peaks in the current traces were difficult to ascertain for voltages around the reversal potential (*triangles*), therefore these times were estimated by extrapolation (*circles*). (*B*) The time-to-peak was then used to program the duration of the depolarizing pulse for each particular voltage, such that the tail current is elicited at the peak of the inward current. Representative traces are shown above the voltage protocol. (*C*) Average tail current amplitudes obtained with this voltage protocol using cells transiently transfected with ($n = 7$).

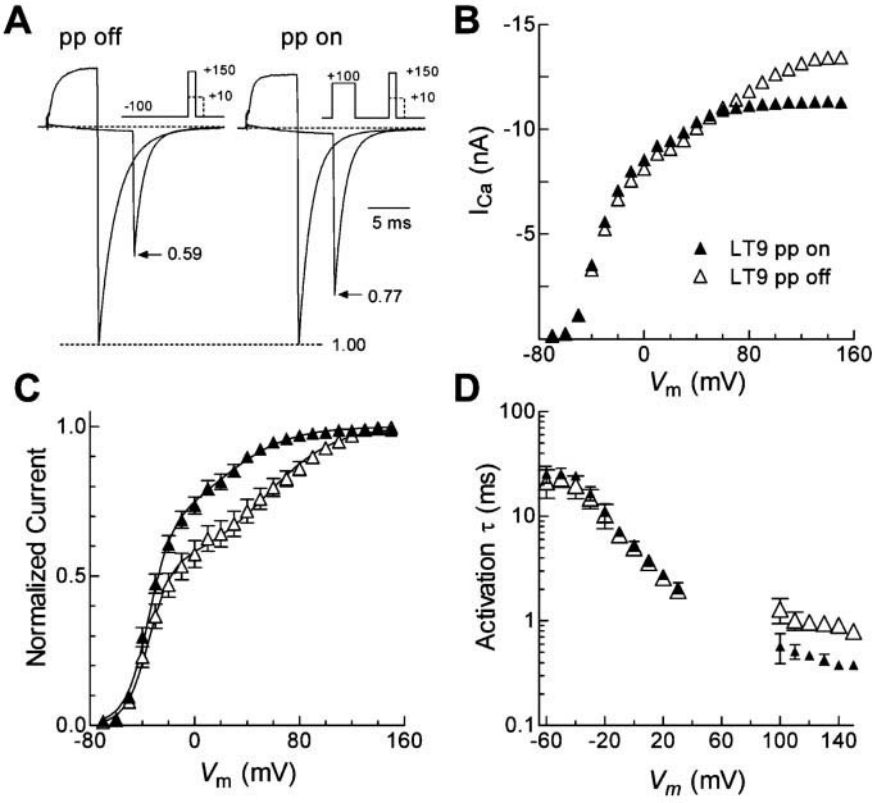

FIGURE 7 A depolarizing prepulse affects $Ca_v3.3$ gating. (*A*) Representative LT9 currents obtained during pulses to +10 and +150 mV before (*left*) and after a prepulse (*right*). Protocol is shown in the inset. The prepulse was 200 ms at +100 mV, and the test pulse was initiated 300 ms later. To illustrate the effect of the prepulse, the data were normalized to the maximum tail current observed under each condition (+150 mV), and the ratio (I_{+10}/I_{+150}) is indicated with an arrow. (*B*) Average tail current amplitudes measured after repolarization to −100 mV from varying test potentials (V_m). Data were obtained for LT9 under control conditions (*open symbols*) or after a prepulse to +100 mV (*closed symbols*). Data represent the average from seven transiently transfected cells. (*C*) The data were normalized to the maximum tail current observed under each condition (+150 mV), then fit with a double Boltzmann function (*smooth curves*). (*D*) Activation kinetics are minimally affected by the prepulse. Currents elicited during the test pulses were fit to a single-exponential function (Chebyshev algorithm, Clampfit). Currents near the reversal potential did not display a clear peak, so activation could not be reliably determined between +40 and +90 mV.

DISCUSSION

Although the cloning of human $Ca_v3.3$ cDNAs has been reported previously (Mittman et al., 1999; Monteil et al., 2000b), we present evidence that these cDNAs were not full-length, and that there is an additional exon that adds 214 amino acids to the carboxyl terminus. The exon structure of human CACNA1I was studied by Mittman et al. using PCR (Mittman et al., 1999). This analysis predicted 36 exons and two sites of alternative splicing: variable inclusion of exon 9 and an alternative acceptor in exon 33. None of the $Ca_v3.3$ cDNAs expressed so far have included exon 9 (Lee et al., 1999; McRory et al., 2001; Monteil et al., 2000b). The human genomic sequence was determined by the Sanger Center Chromosome Mapping Group, and the 5′ end was reported in GenBank entry AL022312 (Dunham et al., 1999). They predicted the existence of an additional 141-bp exon (98612. . .98753) in the 5′ untranslated region, which splices to position −22. The rat cDNA we cloned using conventional cDNA library screening contained 265 bp of 5′ untranslated sequence (Lee et al., 1999). The new 141-bp exon is 79% identical to the rat sequence. However, the rat sequence matches human genomic sequences even further upstream, indicating that the start site of this exon was not correctly identified. The program Promoter 2.0 predicts a transcription start site at 98,400 of AL022312, which is only 91 bp further upstream than predicted by homology to the rat (Knudsen, 1999). We suggest that exon 1 (98400.98753) contributes 353 bp to the 5′ end, bringing the total 5′ untranslated region to 375. This putative promoter site is located in a CpG island. The CACNA1G promoter is also located in a CpG island, and methylation of the cytosines in this region has been observed in various human tumors (Toyota et al., 1999). We conclude that CACNA1I contains two more exons than previously recognized (Mittman et al., 1999).

Inclusion of the amino acids encoded by exon 37 doubles the length of the carboxyl terminus to 489 amino acids, and increases the predicted molecular weight of the protein to 241,240. Therefore, 22% of the channel protein is dedicated to the carboxyl terminus. Similarly, the carboxy terminus of $Ca_v1.2$ (α_{1C}) represents a large fraction (30%) of the total channel protein, and more importantly, it plays a role in modulating channel activity (Peterson et al., 2000). This role was originally deduced from proteolysis studies on native channels (Hescheler and Trautwein, 1988), and then confirmed by truncating the cloned cDNA (Wei et al., 1994). We accidentally prepared truncated $Ca_v3.3$ cDNAs (LT4 and LT6), and then took advantage of these truncations to ask whether the carboxy terminus plays a role in channel activity. These recombinant channels differed in terms of the amount of current they generated and in their ability to be facilitated by a prepulse. The largest current density and largest prepulse facilitation were detected in cells transfected with the full-length construct LT9. Al-

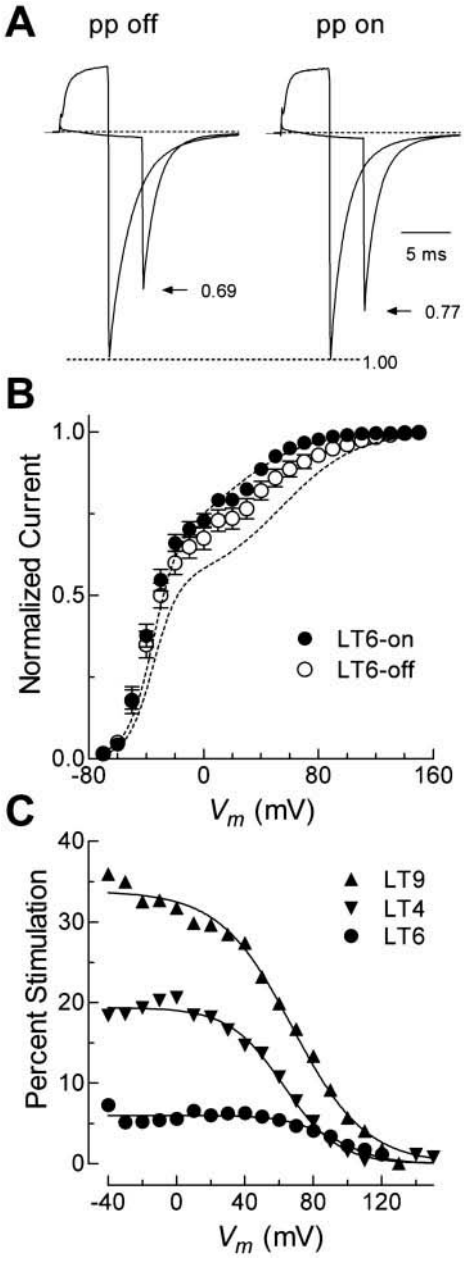

FIGURE 8 Prepulse facilitation is reduced in truncated $Ca_v3.3$ constructs. (*A*) Representative LT6 currents obtained during pulses to +10 and +150 mV (V_m) before (*left*) and after a prepulse (*right*). The protocol is the same as that shown in Fig. 7 *C*. (*B*) Average normalized tail current amplitudes obtained for LT6 under control conditions (*open circles*) or after a prepulse to +100 mV (*filled circles*). Data were obtained from six transiently transfected cells. Dotted curves represent the fit to the LT9 data shown in Fig. 7. (*C*) Stimulation by the prepulse was defined by the increase in the fraction of the normalized tail current at each potential. For example, the data in *A* would correspond to an 11% stimulation. Average results obtained using eight cells transiently transfected with LT4 are also shown. Smooth curves represent fits to the data with a Boltzmann function. Series resistance errors do not appear to affect the results because there was no correlation between the prepulse stimulation and the initial uncompensated series resistance. The peak of the tail current occurred 210 ± 10 μs (n = 7) after the command voltage was changed to +150 mV, providing additional evidence that the clamp was adequate.

though the increased channel expression might be ascribed to the carboxy terminus a strict correlation was not observed, as LT6 produced larger currents than the shorter LT4. The present studies do not rule out a difference in mRNA stability, and it should be noted that there is a stable hairpin structure (nt 6256–6339) that is present in LT6 and LT9, but missing from LT4. The extent of prepulse facilitation did correlate with the size of the carboxy terminus, as channels with shortest carboxy terminus, LT6, had little or no facilitation. The other biophysical properties of LT4, 6, and 9 were nearly identical, with minor differences in the development and recovery from inactivation. Their pharmacological properties are also similar, as both are inhibited to a similar extent by either 0.3 mM Ni^{2+} (LT4, 56 ± 1%, n = 3; LT9, 49 ± 1% inhibition, n = 4) or 3 mM methylphenyl-succinimide (LT4, 62 ± 2%, n = 3; LT9, 58 ± 2% inhibition, n = 5). Monteil et al. also cloned a human $Ca_v3.3$ cDNA that appears to be truncated (Monteil et al., 2000b). The gating of their channel recorded in 2 mM Ca^{2+} is similar to what we obtained in 5 mM Ca^{2+} (Table 1), although minor kinetic differences are noted. We conclude that the distal portion of the carboxy terminus does not play a major role in T-type channel gating, but does play a role in regulation. Chimeric studies where the carboxy termini of the T-type channel $Ca_v3.1$ were replaced with that of the L-type channel $Ca_v1.2$ indicated that inactivation determinants were located close to the IVS6 region (Staes et al., 2001). It is likely that T-type channels are similar to high voltage-activated channels in that many regions are involved in channel inactivation (Hering et al., 2000).

Studies comparing the voltage-dependence of activation of cloned T-type channels have yielded conflicting results. Some studies have concluded that $Ca_v3.3$ gated at less negative potentials than $Ca_v3.1$ (Frazier et al., 2001; Monteil et al., 2000b) and $Ca_v3.2$ (Lee et al., 1999), while others found no difference (Klöckner et al., 1999; Martin et al., 2000). Part of these discrepancies might be explained by the different methods used. Estimates made from *I-V* data yield the most negative values for $V_{1/2}$ because activation at positive potentials is not included. Applying this analysis to our three human channels indicates that they activate at similar potentials (Table 1).

The kinetics of activation, inactivation, and recovery from inactivation determine the channel's response to physiological stimuli. T-type channels are thought to play a central role in mediating burst firing, particularly rebound bursts that occur after an inhibitory post-synaptic potential (IPSP) (Huguenard, 1996). Recovery from inactivation is sufficiently fast that a significant fraction of $Ca_v3.3$ channels should recover after an IPSP. The rate of recovery from inactivation can be used to distinguish the three isotypes of T channels (Klöckner et al., 1999; Satin and Cribbs, 2000), with $Ca_v3.1$ recovering the fastest (Table 1).

Human $Ca_v3.3$ channels close in a biexponential manner, as recently reported for rat $Ca_v3.3a$ (Frazier et al., 2001).

Single channel studies of dorsal root ganglion neurons indicate that at very negative potentials the kinetics of the tail current can be explained by the mean open time (Carbone and Lux, 1987). Recent whole-cell studies on the cloned rat $Ca_v3.3a$ suggest that the slow τ reflects channel activation, or reopening (Frazier et al., 2001). Interestingly, this activation process can be detected at voltages ~20 mV more negative than the inward currents. In neurons such tail currents may elicit an after depolarizing potential, which in turn can trigger burst firing (Higashima et al., 1998; White et al., 1989).

Estimates from tail currents reveal additional activation at positive potentials, suggesting that a fraction of channels do not gate as low voltage-activated channels. Similar bimodal activation has been noted previously for human $Ca_v3.1$ (Monteil et al., 2000a) and $Ca_v3.2$ (Williams et al., 1999), but not $Ca_v3.3$ (Monteil et al., 2000b). Interestingly, we find that a strong depolarizing pulse can increase the fraction of channels in the LVA mode. Strong depolarizing pulses can facilitate the activity of all voltage-activated Ca^{2+} channels. In the case of Ca_v2 channels, this is thought to be due to reversal of G-protein inhibition. The mechanisms by which Ca_v1 channels are regulated by a prepulse remain controversial, although recent evidence supports a direct effect of membrane potential (Kavalali et al., 1997; Kourennyi and Barnes, 2000). Similarly, there is controversy regarding the mechanism(s) by which native T-type channels are regulated by a prepulse, with some evidence supporting prepulse-induced relief of inhibition by a G-protein (Alvarez et al., 1996; Publicover et al., 1995). T-type currents in mouse spermatogenic cells can also be regulated by a prepulse (Arnoult et al., 1997). This study suggested a role for tyrosine phosphorylation, since facilitation was no longer observed in the presence of kinase inhibitors (10 μM tyrphostin A47 or phenylarsine oxide). Sperm appear to predominantly express $Ca_v3.2$ channels (Son et al., 2000). Additional studies are required to determine how human $Ca_v3.3$ channels are regulated, and whether this regulation differs from the rat isoforms. It should be noted that rat $Ca_v3.3$ channels do show some forms of facilitation. Kozlov et al. found that an 8-ms pulse to +50 mV could accelerate the activation kinetics of a second pulse (Kozlov et al., 1999). This effect decayed rapidly, and was gone if the two pulses were separated by >80 ms. The results we present use a 300 ms interval, so this form of regulation lasts longer. Klöckner et al. found more current in the test pulse when a prepulse to +100 mV was given when compared to a prepulse of −30 mV. This type of facilitation took seconds to decay (Klöckner et al., 1999), and is reminiscent of the facilitation measured with native smooth muscle T currents (Ganitkevich and Isenberg, 1991). It is likely that we are measuring the same phenomenon, with the difference being that we do not need to induce inactivation to see the effect of the prepulse. The physiological consequence of facilitation is that $Ca_v3.3$ currents can increase during the early part of a train of action potentials, and this effect should be more pronounced with the human isoforms (Kozlov et al., 1999).

In summary, we have cloned a full-length cDNA that encodes human $Ca_v3.3$ channels. The biophysical properties of the human channel are similar to both truncated versions of the human and to previously cloned rat $Ca_v3.3$ channels. We found evidence for two populations of channels, and show that they could be interconverted with a depolarizing pulse.

We thank Jennifer DeLisle for technical assistance. The Kazusa DNA Research Institute, Chiba, Japan, kindly provided the KIAA1120 cDNA. We thank Glaxo-SmithKline for help with DNA sequencing.

This work was supported by National Institutes of Health Grant NS38691 (to E.P-R.).

REFERENCES

Altschul, S. F., T. L. Madden, A. A. Schaffer, J. Zhang, Z. Zhang, W. Miller, and D. J. Lipman. 1997. Gapped BLAST and PSI-BLAST: a new generation of protein database search programs. *Nucleic Acids Res.* 25:3389–3402.

Alvarez, J. L., L. S. Rubio, and G. Vassort. 1996. Facilitation of T-type calcium current in bullfrog atrial cells: voltage-dependent relief of a G protein inhibitory tone. *J. Physiol. (Lond.).* 491:321–334.

Arnoult, C., J. R. Lemons, and H. M. Florman. 1997. Voltage-dependent modulation of T-type calcium channels by protein tyrosine phosphorylation. *EMBO J.* 16:1593–1599.

Bean, B. P. 1989. Neurotransmitter inhibition of neuronal calcium currents by changes in channel voltage dependence. *Nature.* 340:153–156.

Carbone, E., and H. D. Lux. 1987. Single low-voltage-activated calcium channels in chick and rat sensory neurones. *J. Physiol. (Lond.).* 386: 571–601.

Cribbs, L. L., J. C. Gomora, A. N. Daud, J. H. Lee, and E. Perez-Reyes. 2000. Molecular cloning and functional expression of $Ca_v3.1c$, a T-type calcium channel from human brain [published erratum appears in *FEBS Lett.* 470:378, 2000]. *FEBS Lett.* 466:54–58.

Cribbs, L. L., J. H. Lee, J. Yang, J. Satin, Y. Zhang, A. Daud, J. Barclay, M. P. Williamson, M. Fox, M. Rees, and E. Perez-Reyes. 1998. Cloning and characterization of α_{1H} from human heart, a member of the T-type Ca^{2+} channel gene family. *Circ. Res.* 83:103–109.

Dunham, I., N. Shimizu, B. A. Roe, S. Chissoe, A. R. Hunt, J. E. Collins, R. Bruskiewich, D. M. Beare, M. Clamp, L. J. Smink, R. Ainscough, J. P. Almeida, A. Babbage, C. Bagguley, J. Bailey, K. Barlow, K. N. Bates, O. Beasley, C. P. Bird, S. Blakey, A. M. Bridgeman, D. Buck, J. Burgess, W. D. Burrill, K. P. O'Brien, et al. 1999. The DNA sequence of human chromosome 22. *Nature.* 402:489–495.

Ertel, E., K. Campbell, M. M. Harpold, F. Hofmann, Y. Mori, E. Perez-Reyes, A. Schwartz, T. Snutch, T. Tanabe, L. Birnbaumer, R. W. Tsien, and W. A. Catterall. 2000. Nomenclature of voltage-gated calcium channels. *Neuron.* 25:533–535.

Frazier, C. J., J. R. Serrano, E. G. George, X. Yu, A. Viswanathan, E. Perez-Reyes, and S. W. Jones. 2001. Gating kinetics of the α_{1I} T-type calcium channel. *J. Gen. Physiol.* 118:457–470.

Ganitkevich, V., and G. Isenberg. 1991. Stimulation-induced potentiation of T-type Ca^{2+} channel currents in myocytes from guinea-pig coronary artery. *J. Physiol. (Lond.).* 443:703–725.

Gomora, J. C., A. N. Daud, N. C. McNaughton, A. L. Medhurst, P. J. Green, M. N. Pangalos, A. Randall, and E. Perez-Reyes. 2000. Cloning, distribution, and functional expression of a human a1I low voltage-activated Ca channel. *Soc. Neurosci. Abstr.* 26:365.

Hering, S., S. Berjukow, S. Sokolov, R. Marksteiner, R. G. Weiss, R. Kraus, and E. N. Timin. 2000. Molecular determinants of inactivation in voltage-gated Ca^{2+} channels. *J. Physiol. (Lond.).* 528:237–249.

Hescheler, J., and W. Trautwein. 1988. Modification of L-type calcium current by intracellularly applied trypsin in guinea-pig ventricular myocytes. *J. Physiol. (Lond.).* 404:259–274.

Higashima, M., H. Kinoshita, and Y. Koshino. 1998. Contribution of T-type calcium channels to after-discharge generation in rat hippocampal slices. *Brain Res.* 781:127–134.

Huguenard, J. R. 1996. Low threshold calcium currents in central nervous system neurons. *Annu. Rev. Physiol.* 58:329–348.

Huguenard, J. R., M. J. Gutnick, and D. A. Prince. 1993. Transient Ca^{2+} currents in neurons isolated from rat lateral habenula. *J. Neurophysiol.* 70:158–166.

Huguenard, J. R., and D. A. Prince. 1992. A novel T-type current underlies prolonged Ca^{2+}-dependent burst firing in GABAergic neurons of rat thalamic reticular nucleus. *J. Neurosci.* 12:3804–3817.

Kavalali, E. T., K. S. Hwang, and M. R. Plummer. 1997. cAMP-dependent enhancement of dihydropyridine-sensitive calcium channel availability in hippocampal neurons. *J. Neurosci.* 17:5334–5348.

Klöckner, U., J. H. Lee, L. L. Cribbs, A. Daud, J. Hescheler, A. Pereverzev, E. Perez-Reyes, and T. Schneider. 1999. Comparison of the Ca^{2+} currents induced by expression of three cloned α_1 subunits, α_{1G}, α_{1H} and α_{1I}, of low-voltage-activated T-type Ca^{2+} channels. *Eur. J. Neurosci.* 11:4171–4178.

Knudsen, S. 1999. Promoter 2.0: for the recognition of PolII promoter sequences. *Bioinformatics.* 15:356–361.

Kourennyi, D. E., and S. Barnes. 2000. Depolarization-induced calcium channel facilitation in rod photoreceptors is independent of G proteins and phosphorylation. *J. Neurophysiol.* 84:133–138.

Kozlov, A. S., F. McKenna, J. H. Lee, L. L. Cribbs, E. Perez-Reyes, A. Feltz, and R. C. Lambert. 1999. Distinct kinetics of cloned T-type Ca^{2+} channels lead to differential Ca^{2+} entry and frequency-dependence during mock action potentials. *Eur. J. Neurosci.* 11:4149–4158.

Kuo, C. C., and S. Yang. 2001. Recovery from inactivation of T-type Ca^{2+} channels in rat thalamic neurons. *J. Neurosci.* 21:1884–1892.

Lee, J. H., A. N. Daud, L. L. Cribbs, A. E. Lacerda, A. Pereverzev, U. Klöckner, T. Schneider, and E. Perez-Reyes. 1999. Cloning and expression of a novel member of the low voltage-activated T-type calcium channel family. *J. Neurosci.* 19:1912–1921.

Liman, E. R., J. Tytgat, and P. Hess. 1992. Subunit stoichiometry of a mammalian K+ channel determined by construction of multimeric cDNAs. *Neuron.* 9:861–871.

Martin, R. L., J. H. Lee, L. L. Cribbs, E. Perez-Reyes, and D. A. Hanck. 2000. Mibefradil block of cloned T-type calcium channels. *J. Pharmacol. Exp. Ther.* 295:302–308.

McRory, J. E., C. M. Santi, K. S. Hamming, J. Mezeyova, K. G. Sutton, D. L. Baillie, A. Stea, and T. P. Snutch. 2001. Molecular and functional characterization of a family of rat brain T-type calcium channels [published erratum appears in *J. Biol. Chem.* 276:30571–30574, 2001]. *J. Biol. Chem.* 276:3999–4011.

Mittman, S., J. Guo, M. C. Emerick, and W. S. Agnew. 1999. Structure and alternative splicing of the gene encoding α_{1I}, a human brain T calcium channel α_1 subunit. *Neurosci. Lett.* 269:121–124.

Monteil, A., J. Chemin, E. Bourinet, G. Mennessier, P. Lory, and J. Nargeot. 2000a. Molecular and functional properties of the human α1G subunit that forms T-type calcium channels. *J. Biol. Chem.* 275: 6090–6100.

Monteil, A., J. Chemin, V. Leuranguer, C. Altier, G. Mennessier, E. Bourinet, P. Lory, and J. Nargeot. 2000b. Specific properties of T-type calcium channels generated by the human α1I subunit. *J. Biol. Chem.* 275:16530–16535.

Murbartián, J., J. C. Gomora, and E. Perez-Reyes. 2002. Electrophysiological characterization of two new isoforms of rat $Ca_v3.3$ T-type calcium channel. *Biophys. J.* 82:99*a*. (Abstr.).

Pan, Z. H. 2000. Differential expression of high- and two types of low-voltage-activated calcium currents in rod and cone bipolar cells of the rat retina. *J. Neurophysiol.* 83:513–527.

Perez-Reyes, E., L. L. Cribbs, A. Daud, A. E. Lacerda, J. Barclay, M. P. Williamson, M. Fox, M. Rees, and J-H. Lee. 1998. Molecular characterization of a neuronal low voltage-activated T-type calcium channel. *Nature.* 391:896–900.

Peterson, B. Z., J. S. Lee, J. G. Mulle, Y. Wang, M. de Leon, and D. T. Yue. 2000. Critical determinants of Ca^{2+}-dependent inactivation within an EF-hand motif of L-type Ca^{2+} channels. *Biophys. J.* 78:1906–1920.

Publicover, S. J., M. R. Preston, and A. J. El Haj. 1995. Voltage-dependent potentiation of low-voltage-activated Ca^{2+} channel currents in cultured rat bone marrow cells. *J. Physiol. (Lond.).* 489:649–661.

Randall, A. D., and R. W. Tsien. 1997. Contrasting biophysical and pharmacological properties of T- type and R-type calcium channels. *Neuropharmacology.* 36:879–893.

Satin, J., and L. L. Cribbs. 2000. Identification of a T-type Ca^{2+} channel isoform in murine atrial myocytes (AT-1 cells). *Circ. Res.* 86:636–642.

Serrano, J. R., E. Perez-Reyes, and S. W. Jones. 1999. State-dependent inactivation of the α1G T-type calcium channel. *J. Gen. Physiol.* 114: 185–201.

Son, W. Y., J. H. Lee, and C. T. Han. 2000. Acrosome reaction of human spermatozoa is mainly mediated by α1H T-type calcium channels. *Mol. Hum. Reprod.* 6:893–897.

Staes, M., K. Talavera, N. Klugbauer, J. Prenen, L. Lacinová, G. Droogmans, F. Hofmann, and B. Nilius. 2001. The amino side of the C-terminus determines fast inactivation of the T-type calcium channel α_{1G}. *J. Physiol. (Lond.).* 530:35–45.

Talley, E. M., L. L. Cribbs, J. H. Lee, A. Daud, E. Perez-Reyes, and D. A. Bayliss. 1999. Differential distribution of three members of a gene family encoding low voltage-activated (T-type) calcium channels. *J. Neurosci.* 19:1895–1911.

Tarasenko, A. N., P. G. Kostyuk, A. V. Eremin, and D. S. Isaev. 1997. Two types of low-voltage-activated Ca^{2+} channels in neurones of rat laterodorsal thalamic nucleus. *J. Physiol. (Lond.).* 499:77–86.

Toyota, M., C. Ho, M. Ohe-Toyota, S. B. Baylin, and J. P. Issa. 1999. Inactivation of *CACNA1G*, a T-type calcium channel gene, by aberrant methylation of its 5′ CpG island in human tumors. *Cancer Res.* 59: 4535–4541.

Wei, X. Y., A. Neely, A. E. Lacerda, R. Olcese, E. Stefani, E. Perez-Reyes, and L. Birnbaumer. 1994. Modification of Ca^{2+} channel activity by deletions at the carboxyl terminus of the cardiac α_1 subunit. *J. Biol. Chem.* 269:1635–1640.

White, G., D. M. Lovinger, and F. F. Weight. 1989. Transient low-threshold Ca^{2+} current triggers burst firing through an after-depolarizing potential in an adult mammalian neuron. *Proc. Natl. Acad. Sci. U.S.A.* 86:6802–6806.

Williams, M. E., M. S. Washburn, M. Hans, A. Urrutia, P. F. Brust, P. Prodanovich, M. M. Harpold, and K. A. Stauderman. 1999. Structure and functional characterization of a novel human low-voltage activated calcium channel. *J. Neurochem.* 72:791–799.